Title	Theoretical and Kinetic Study of the Reaction of Ethyl Methyl Ketone with HO2 for T = 600 -1, 600 K. Part II: Addition Reaction Channels
Author(s)	Zhou, Chong-Wen; Mendes, Jorge; Curran, Henry J.
Publication Date	2013
Publication Information	Zhou, Chong-Wen, Mendes, Jorge, & Curran, Henry J. (2013). Theoretical and Kinetic Study of the Reaction of Ethyl Methyl Ketone with H2 for T = 600–1600 K. Part II: Addition Reaction Channels. The Journal of Physical Chemistry A, 117(22), 4526-4533. doi: 10.1021/jp3128127
Link to publisher's version	http://pubs.acs.org/doi/abs/10.1021/jp3128127
Item record	http://hdl.handle.net/10379/3412

Theoretical and Kinetic Study of the Reaction of Ethyl Methyl Ketone with $H\dot{O}_2$ for $T = 600 - 1,600$ K. Part II: Addition Reaction Channels

Chong-Wen Zhou*, Jorge Mendes, Henry J. Curran

Combustion Chemistry Centre,
National University of Ireland, Galway, Ireland.

May 9, 2013

* To whom correspondence should be addressed. E-mail: chongwen.zhou@nuigalway.ie

Abstract

The temperature and pressure dependence of the addition reaction of ethyl methyl ketone (EMK) with $H\dot{O}_2$ radical has been calculated using the master equation method employing conventional transition state theory estimates for the microcanonical rate coefficients in the temperature range of 600–1600 K. Geometries, frequencies, and hindrance potentials were obtained at the B3LYP/6-311G(d,p) level of theory. A modified G3(MP2,CC) method has been used to calculate accurate electronic energies for all of the species involved in the reactions. The rigid-rotor harmonic oscillator approximation has been used for all of the vibrations except for the torsional degrees of freedom which are being treated as 1D hindered rotors. Asymmetric Eckart barriers were used to model tunneling effect in a one-dimensional reaction coordinate through saddle points. Our calculated results show that the four reaction channels forming 1-buten-2-ol + $H\dot{O}_2$ radical (R5), 2-buten-2-ol + $H\dot{O}_2$ radical (R10), acetic acid + ethylene + $\dot{O}H$ radical (R13), 2-methyl-2-oxetanol + $\dot{O}H$ radical (R15) are the dominant channels. When the temperature is below 1000 K, the reaction R15 forming the cyclic ether, 2-methyl-2-oxetanol, is dominant; while the reaction R13 forming acetic acid + ethylene + $\dot{O}H$ radical becomes increasingly dominant at temperatures above 1000 K. The other two channels forming 1-buten-2-ol, 2-buten-2-ol and $H\dot{O}_2$ radical are not dominant but are still important product channels over the whole temperature range investigated here. No pressure dependence has been found for the reaction channels forming 2-methyl-2-oxetanol + $\dot{O}H$ radical and acetic acid + ethylene + $\dot{O}H$ radical. A slightly negative pressure dependence has been found for the reaction channels producing the two butenols. Rate constants for the four important reaction channels at 1 atm (in $cm^3mol^{-1}s^{-1}$) are:

$$
\begin{aligned}
k_{\mathrm{R5}} &= 2.67 \times 10^{15} \times T^{-1.32} \exp(-16637/T) \\
k_{\mathrm{R10}} &= 1.62 \times 10^{8} \times T^{0.57} \exp(-13142/T) \\
k_{\mathrm{R13}} &= 2.29 \times 10^{17} \times T^{-1.66} \exp(-18169/T) \\
k_{\mathrm{R15}} &= 6.17 \times 10^{-2} \times T^{3.35} \exp(-10136/T)
\end{aligned}
$$

A comparison of the total rate constants for the addition of $H\dot{O}_2$ radical to EMK and that for H-atom abstraction by $H\dot{O}_2$ radical from EMK has also been carried out. We find that the abstraction reaction channels are dominant over the entire temperature range of 600–1600 K.

Keywords

ab initio, 1-buten-2-ol, 2-buten-2-ol, acetic acid, cyclic ether

1 Introduction

Oxygenated hydrocarbons (involving different kinds of C–O bonds, like aldehydes, ethers, alcohols, ketones, esters, etc.) are implicated in the combustion process of several fossil fuels either as additives or as stable intermediate species. Two issues associated with oxygen-containing fuels are their ability to reduce particulate emissions like NO,[1] and their propensity to form toxic byproducts such as aldehydes.[2] A fundamental understanding of oxygenate combustion chemistry is necessary to fully exploit the former and minimize the latter. Moreover, the hierarchical nature of hydrocarbon oxidation implies that simpler oxygenates, play a vital role in the accurate combustion modeling of a wide range of components of practical fuels. A detailed investigation of the combustion properties of such small oxygenated fuels or intermediates is important in predicting the chemical kinetics of larger oxygenated species.

Ethyl methyl ketone (EMK) has been detected as a common oxygenated intermediate in the combustion of alcohols like *n*-propanol and *i*-propanol,[3] and its reaction with $\dot{O}H$ radical has been investigated recently.[4] Hydroperoxy radicals ($H\dot{O}_2$) are particularly important species at intermediate temperatures, as they lead to the formation of $\dot{O}H$ radicals through the H-atom abstraction reaction process in which one $H\dot{O}_2$ radical generates three radicals (two $\dot{O}H$ radicals and one other) which greatly contribute to chain branching. Even though, the reactions of $H\dot{O}_2$ radical with RH is typically slow, while the concentration of the $H\dot{O}_2$ radical is usually significantly higher than that of the $\dot{O}H$ radical in the intermediate temperature ignition process, so the above reactions have a large effect on the chemistry.

The kinetics of H-atom abstraction by $H\dot{O}_2$ radical from EMK has been investigated recently by our group,[5] and the reactivity comparison with alkanes was also presented. In addition to the H-atom abstraction reaction, we found that the addition channel of $H\dot{O}_2$ radical to the C=O in EMK has much lower barrier height than the direct H-atom abstraction process, so it is also interesting to compare the competitive between these two different reaction mechanism.

This work focuses on investigating the chemical kinetics of the addition reaction of $H\dot{O}_2$

radical to EMK to form an alcoholic alkyl peroxy radical ($\mathrm{RO\dot{O}}$), together with its subsequent isomerization reactions to form different alcoholic alkyl hydroperoxy radical isomers ($\mathrm{\dot{Q}OOH}$) and their β-scission reactions and cyclic ether formation reactions *etc*. Depending upon the temperature and pressure, this sequence of reactions can either accelerate or decelerate the overall ignition kinetics. With an initial addition reaction of,

$$\mathrm{H\dot{O}_2 + CH_3C(O)CH_2CH_3 \rightarrow CH_3C(O\dot{O})OHCH_2CH_3} \quad \text{(R1)}$$

the $\mathrm{CH_3C(O\dot{O})OHCH_2CH_3}$ ($\mathrm{RO\dot{O}}$) producted can isomerize to $\mathrm{\dot{C}H_2COOHOHCH_2CH_3}$ (α_p-$\mathrm{\dot{Q}OOH}$), $\mathrm{CH_3COOHOH\dot{C}HCH_3}$ (α_s-$\mathrm{\dot{Q}OOH}$) and $\mathrm{CH_3COOHOHCH_2\dot{C}H_2}$ (β-$\mathrm{\dot{Q}OOH}$) through inter-molecular H-atom transfer reactions.

It is also interesting to find that the $\mathrm{RO\dot{O}}$ radical formed is also a very important intermediate in the oxidation of *sec*-butanol which is generated in the following sequence of reactions:

$$\mathrm{CH_3CHOHCH_2CH_3} \xrightarrow[\text{by } \dot{\mathrm{O}}\mathrm{H},\ \dot{\mathrm{H}},\ \mathrm{H\dot{O}_2}\ \textit{etc}]{\text{H}-\text{abstraction}} \mathrm{CH_3\dot{C}OHCH_2CH_3} \quad \text{(R2)}$$

$$\mathrm{CH_3\dot{C}OHCH_2CH_3 + O_2 \rightarrow CH_3C(O\dot{O})OHCH_2CH_3} \quad \text{(R3)}$$

Thus, clearly describing the decomposition kinetics of $\mathrm{CH_3C(O\dot{O})OHCH_2CH_3}$ is also important in understanding the low-temperature chemistry of the oxidation of *sec*-butanol.

It is well known that the low-temperature oxidation of hydrocarbon fuels is largely governed by the reactions of alkyl peroxy radicals ($\mathrm{RO\dot{O}}$) and their hydroperoxy alkyl radical isomers ($\mathrm{\dot{Q}OOH}$) which can add to $\mathrm{O_2}$ or can decompose to produce cyclic ethers, carbonyl compounds, olefins *etc*. In this work, the reactions under investigation is shown in Fig. 1 and the reaction pathways are summarized as follows:

$$
\begin{aligned}
\mathrm{CH_3COCH_2CH_3 + H\dot{O}_2} &\rightarrow \mathrm{CH_3C(O\dot{O})OHCH_2CH_3} & & \\
\mathrm{CH_3C(O\dot{O})OHCH_2CH_3} &\rightleftharpoons \mathrm{\dot{C}H_2COOHOHCH_2CH_3} &\rightarrow \mathrm{CH_2{=}COHOOH + \dot{C}H_2CH_3} & \text{(R4)}\\
& &\rightarrow \mathrm{CH_2{=}COHCH_2CH_3 + H\dot{O}_2} & \text{(R5)}\\
& &\rightarrow \mathrm{CH_3CH_2COCH_2OH + \dot{O}H} & \text{(R6)}\\
& &\rightarrow \mathrm{CH_2OCOHCH_2CH_3 + \dot{O}H} & \text{(R7)}\\
\mathrm{CH_3C(O\dot{O})OHCH_2CH_3} &\rightleftharpoons \mathrm{CH_3COOHOH\dot{C}HCH_3} &\rightarrow \mathrm{CH_3CH{=}COHOOH + \dot{C}H_3} & \text{(R8)}\\
& &\rightarrow \mathrm{CH_2{=}CHCOHOOHCH_3 + \dot{H}} & \text{(R9)}\\
& &\rightarrow \mathrm{CH_3COH{=}CHCH_3 + H\dot{O}_2} & \text{(R10)}\\
& &\rightarrow \mathrm{CH_3CHOHCOCH_3 + \dot{O}H} & \text{(R11)}\\
& &\rightarrow \mathrm{CH_3COHOCHCH_3 + \dot{O}H} & \text{(R12)}\\
\mathrm{CH_3C(O\dot{O})OHCH_2CH_3} &\rightleftharpoons \mathrm{CH_3COOHOHCH_2\dot{C}H_2} &\rightarrow \mathrm{CH_3COOH + C_2H_4 + \dot{O}H} & \text{(R13)}\\
& &\rightarrow \mathrm{CH_3COHOOHCH{=}CH_2 + \dot{H}} & \text{(R14)}\\
& &\rightarrow \mathrm{CH_3COHOCH_2CH_2 + \dot{O}H} & \text{(R15)}
\end{aligned}
$$

2 Computational methods

2.1 Potential energy surface calculations

The geometries of reactants, transition states, intermediates and products of the title reaction have been optimized using the hybrid density function theory B3LYP method with the 6-311G(d,p) basis set.[6] Vibrational frequencies, molecular structural parameters, zero-point corrections and the hindrance potentials for the 1D hindered rotors are all obtained at the same level of theory. The intrinsic reaction coordinate (IRC)[7] calculations were carried out to validate some important connections between transition states and local minima.

The final G3(MP2,CC)//B3LYP version[8] for the high-level single-point energy calculations was used to obtain more accurate electronic energies for all species. The final total energies at 0 K obtained by using the B3LYP optimized geometries were computed as follows:

$$\mathrm{E_0[G3(MP2,CC)] = E[RCCSD(T)/6-311G(d,p)] + \Delta E_{MP2} + \Delta E(SO) + \Delta E(HLC) + E(ZPE)}$$

where $\Delta E_{MP2} = E[MP2/G3large] - E[MP2/6-311G(d,p)]$ is the basis set correction, $\Delta E(SO)$ is a spin-orbit correction (not included in our calculation); the high level correction, $\Delta E(HLC)$ was also omitted in our calculations because in most cases the isomerization of radical species considered here proceed without a spin change, resulting in HLC cancellation. Otherwise, neglecting HLC may introduce an error of 2–3 kcal mol^{-1}. Since the scaling of the ZPE does not significantly affect the relative energies of isomers and transition states, the unscaled ZPE was used in this calculation. Vibrational frequencies with a scaling factor of 0.9682 was used in the rate constants calculations. The Gaussian 09 program package[9] has been used to perform the B3LYP geometry optimization, frequency calculations, the hindrance potential in addition to the MP2 single-point energy calculations, whereas the MOLPRO 2010 code[10] was employed to perform calculations of RHF-RCCSD(T) spin-restricted coupled cluster energies.

2.2 Rate constant calculations

Temperature and pressure-dependent rate constants were obtained from the solution of the 1D master equation using the methods developed by Klippenstein and Miller[11,12]on the basis of eigenvalue-eigenvector analysis. The low-frequency torsional modes were treated as 1D hindered rotors using a Pitzer-Gwinn-like approximation. The hindrance potentials were determined for every geometry around every possible dihedral angle by fitting Fourier series to the B3LYP/6-311G(d,p) energies along the relaxed internal rotation. The remaining modes were treated as rigid-rotor harmonic oscillators. Asymmetric Eckart tunneling corrections[13] were included. Collision rates were calculated using the Lennard-Jones potential parameters of $CH_3CO_2C_2H_5$[14] to represent the additional complex with σ=5.65 Å, ϵ=372 K. The bath gas was N_2.[14] The collisional energy transfer probabilities for deactivating collisions were modeled using the single exponential down model, with the average downwards energy transfer parameter assumed to have a temperature dependence given by $< \Delta E_d >= 200(T/298)^{0.85}$ cm^{-1}.[15] Variflex (v2.02m)[16]was used to carry out the rate constant calculations.

3 Results and discussion

3.1 Potential energy diagrams and reaction mechanisms

Potential energy diagrams for the formation of α_p-, α_s- and β-$\dot{Q}$OOH and their subsequent decomposition reactions are shown in Figs. 2, 3 and 4, respectively. Even though the hydrogen bond product complexes have been located in the reaction processes forming $\dot{O}H$ and $H\dot{O}_2$ radicals, they are not included in these figures for simplicity. Cartesian coordinates of the reactant, important transition states, and products are presented in the Supporting Information together with the T1 diagnostics which are much lower than 0.02, indicating that the single-reference method gives an adequate description of the wave function. Rotational symmetry numbers and the optical isomers used in the rate constants calculations are also provided in the Supporting Information.

As shown in Figs. 2, 3, and 4, when the $H\dot{O}_2$ radical approaches EMK, a pre-reaction complex (**RC**) is first formed, which lies 8.6 kcal mol^{-1} below the reactants, then overcoming the submerged transition state, TS1, lying 2.1 kcal mol^{-1} below the reactants to form the alcoholic alkyl peroxy radical RO$\dot{O}$. Over the temperature range of interest here, the formation of the **RC** will slightly enhance the tunneling effect by narrowing the width of the Eckart barrier; the flux through the inner transition state (TS1) is smaller than flux through the barrierless outer transition state leading to the **RC**. Thus, it is of no value to carry out the variational transition state calculations for this barrierless entrance channel since the inner transition state barrier dominates.

Through internal H-atom transfer the formed RO$\dot{O}$ radical can isomerize to α_p-$\dot{Q}$OOH with a barrier height of 35.9 kcal mol^{-1}, Fig. 2; it can form α_s-$\dot{Q}$OOH with a barrier height of 34.1 kcal mol^{-1}, Fig. 3 and it can also form β-$\dot{Q}$OOH with a barrier height of 25.8 kcal mol^{-1}, Fig. 4. Then through different types of decomposition reactions, such as β-scission and cyclic ether formation, these species can go on to form different type of radicals via chain propagation reactions. Detailed information can be obtained in the potential energy diagrams

of Figs. 2, 3 and 4. One interesting thing has been found in the β-scission of α_p-$\dot{Q}$OOH and α_s-$\dot{Q}$OOH to form the $\dot{O}$H radical and relatively stable molecules, through TS2c and TS3d respectively, whose geometries are shown in Fig. 5. Taking the $\dot{O}$H-elimination reaction of α_p-$\dot{Q}$OOH for example, the originally eliminated OH group is O5-H14 in TS2c, while when we made the bond length of C2-O5 in TS2c longer by 20% to try to get the product complex, we found the O5-H14 group remoted towards and finally attached to the unsaturated C1; on the other hand, the O15-O16 bond breaks to form an $\dot{O}$H radical and 1-hydroxy-2-butanone. A similar process has also been found between TS3d and PC3d, shown in Fig. 5, in the $\dot{O}$H-elimination reaction from α_s-$\dot{Q}$OOH. The IRC calculations cannot capture these processes. The $\dot{Q}$OOH intermediates formed with high relative energies are expected to be short-lived.

3.2 Rate constants and product branching ratios

Bimolecular rate constants at 1 atm forming the different products through reaction channels R4 to R15 are shown in Figs. 6, 7, and 8. From Fig. 6 whose products are all from the decomposition of α_p-$\dot{Q}$OOH, we find that the rate constants forming 1-buten-2-ol and the $H\dot{O}_2$ radical are over one order of magnitude faster than the other three channels over the complete temperature range investigated here. The same trend has also been found in the products formation of the decomposition of α_s-$\dot{Q}$OOH shown in Fig. 7; it is clear that rate constants forming 2-buten-2-ol and the $H\dot{O}_2$ radical are also over one order of magnitude faster than the other four reaction channels.

In the decomposition of β-$\dot{Q}$OOH, Fig. 8, the two reaction channels forming the cyclic ether, 2-methyl-2-oxetanol, with the $\dot{O}$H radical and acetic acid + ethylene + $\dot{O}$H radical are competitive with each other and they are both much faster than the other channel forming 2-hydroperoxy-3-buten-2-ol and a $\dot{H}$ atom. When the temperature is lower than 1000 K, the formation of the cyclic ether, 2-methyl-2-oxetanol, is more competitive, whereas when the temperature is above 1000 K, the formation of acetic acid + ethylene + $\dot{O}$H radical becomes increasingly important.

As a summary, the four reaction channels forming 1-buten-2-ol + $H\dot{O}_2$ radical, 2-buten-2-ol + $H\dot{O}_2$ radical, 2-methyl-2-oxetanol + $\dot{O}H$ radical, acetic acid + ethylene + $\dot{O}H$ radical, are much more competitive than the other channels; thus a branching ratio comparison at 1 atm has only been carried out comparing these four channels as shown in Fig. 9. We can see that when the temperature is lower than 1000 K, the formation of 2-methyl-2-oxetanol + $\dot{O}H$ radical is dominant; its branching ratio decreases from 68.6% at 600 K, to 30.1% at 1000 K, and then decreases to 20.4% at 1600 K. On the other hand, the pathway forming acetic acid + ethylene + $\dot{O}H$ radical becomes increasingly dominant at temperatures above 1000 K, increasing gradually from 4.8% at 600 K, to 33.5% at 1000 K and finally becoming 42.0% at 1600 K. The other two butenols formation channels of 1-buten-2-ol + $H\dot{O}_2$ radical and 2-buten-2-ol + $H\dot{O}_2$ radical are not dominant over the whole temperature range but are still important. The branching ratio for the formation of 1-buten-2-ol and $H\dot{O}_2$ radical increases from 5.7% at 600 K, to 18.7% at 1000 K, and then decreases slowly to 17.5% at 1600 K. The branching ratio for the formation of the other butenol, 2-buten-2-ol and $H\dot{O}_2$ radical, increases from 20.9% at 600 K, to 23.1% at 800 K, and then decreases to 10.5% at 1600 K. These four reaction channels are labeled in color in Fig. 1 together with their flux analyses based on rate constants calculated at 1000 K. Through the branching ratio analysis we find that the formation of 2-methyl-2-oxetanol, ethylene, acetic acid, butenols of 2-buten-2-ol and 1-buten-2-ol, $\dot{O}H$ and $H\dot{O}_2$ radicals are important intermediates in the combustion process of alcohols, and this is especially true for *sec*-butanol. The formation of 1-buten-2-ol and 2-buten-2-ol have been detected by Wang *et al.*[17] in the oxidation of the four butanol isomers.

As we mentioned above, no pressure dependence has been found for the reaction channels forming 2-methyl-2-oxetanol + $\dot{O}H$ radical and acetic acid + ethylene + $\dot{O}H$ radical. A slightly negative pressure dependence has been found for the two butenols formation channels. Rate constants at pressures of the collision-less limit, 0.01, 0.1, 1 and 10 atm for the two butenols formation reactions are shown in Figs. 10 and 11. We can see that rate constants of these two channels decrease as the pressure increases, because the physical collision sta-

bilization process forming the wells of α_p-$\dot{Q}$OOH and α_s-$\dot{Q}$OOH becoming competitive with increasing pressure.

The total and individual rate constants of reactions R4–R15 have been fitted to three-parameter Arrhenius-type expressions, valid over the temperature range 600–1600 K at 1 atm with the following results (in $cm^3mol^{-1}s^{-1}$):

$$k_t = 8.09 \times T^{3.04} \exp(-11647/T)$$

$$k_{R4} = 2.47 \times 10^6 \times T^{1.57} \exp(-20960/T)$$

$$k_{R5} = 2.67 \times 10^{15} \times T^{-1.32} \exp(-16637/T)$$

$$k_{R6} = 1.19 \times 10^4 \times T^{1.72} \exp(-17656/T)$$

$$k_{R7} = 3.70 \times 10^5 \times T^{1.53} \exp(-17835/T)$$

$$k_{R8} = 1.40 \times 10^2 \times T^{2.55} \exp(-20422/T)$$

$$k_{R9} = 2.64 \times 10^{-3} \times T^{4.07} \exp(-19723/T)$$

$$k_{R10} = 1.62 \times 10^8 \times T^{0.57} \exp(-13142/T)$$

$$k_{R11} = 1.10 \times 10^{-4} \times T^{3.96} \exp(-16729/T)$$

$$k_{R12} = 6.94 \times 10^{-1} \times T^{2.83} \exp(-15292/T)$$

$$k_{R13} = 2.29 \times 10^{17} \times T^{-1.66} \exp(-18169/T)$$

$$k_{R14} = 3.18 \times 10^3 \times T^{2.70} \exp(-21840/T)$$

$$k_{R15} = 6.17 \times 10^{-2} \times T^{3.35} \exp(-10136/T)$$

A comparison of the total rate constants for the addition of $H\dot{O}_2$ radical to EMK and that for H-atom abstraction by $H\dot{O}_2$ radical from EMK in our recent work[5] is shown in Fig. 12. It is clear that in the temperature range of 600–1600 K, abstraction reactions are over two orders of magnitude faster than the addition reactions. Even though the addition

channel forming the ROȮ radical is almost barrierless, the subsequent isomerization and decomposition reaction channels which have much higher barrier heights compared to the abstraction reaction channels, decrease the reactivity of the addition reaction processes.

4 Conclusions

Bimolecular addition rate constants of $H\dot{O}_2$ radical with ethyl methyl ketone have been calculated in the temperature range of 600 to 1600 K with the master equation method employing conventional transition state theory for the microcanonical rate constants. Geometries, frequencies and hindrance potentials were obtained at the B3LYP/6-311G(d,p) level of theory. A modified G3(MP2,CC) method has been used to calculate the electronic energies for all the species invloved in the reactions. The rigid-rotor harmonic oscillator approximation has been used for all the vibrations but the torsional degrees of freedom which are being treated as 1D hindered rotor.

A comparison of the calculated rate constants shows that four reaction channels forming 1-buten-2-ol + $H\dot{O}_2$ radical, 2-buten-2-ol + $H\dot{O}_2$ radical, 2-methyl-2-oxetanol + $\dot{O}H$ radical, acetic acid + ethylene + $\dot{O}H$ radical are the most important reaction channels. Branching ratio analysis shows that when temperature is lower than 1000 K, the formation of the cyclic ether, 2-methyl-2-oxetanol, is dominant; its branching ratio decreases from 68.6% at 600 K to 30.1 % at 1000 K, and then decreases to 20.4% at 1600 K. While the reaction channel forming acetic acid + ethylene + $\dot{O}H$ radical becomes increasingly dominant when the temperature is greater than 1000 K, whose branching ratio increases from 4.8% at 600 K to 33.5% at 1000 K and finally becomes 42.0% at 1600 K. The other two channels forming $H\dot{O}_2$ radical and the butenols, 1-buten-2-ol and 2-buten-2-ol, are not dominant but are still very important over the entire temperature range we investigated here. The branching ratio for the channel forming 1-buten-2-ol and $H\dot{O}_2$ radical increases from 5.7% at 600 K to 18.7% at 1000 K and then decreases gradually to 17.5% at 1600 K; while the branching ratio for the formation of

$H\dot{O}_2$ radical and the other butenol of 2-buten-2-ol increases from 20.9% at 600 K to 23.1% at 800 K and then decreases to 10.5% at 1600 K.

No pressure dependence has been found for the reaction channels forming 2-methyl-2-oxetanol + $\dot{O}H$ radical and acetic acid + ethylene + $\dot{O}H$ radical. Slightly negative pressure dependence for the formation of the two butenol reaction channels has been found. Fitted modified Arrhenius expressions for the rate constants of all of the reaction channels (R4 – R15) at 1 atm have been provided in the paper.

A comparison of the total rate constants for the addition of $H\dot{O}_2$ radical to EMK and that for H-atom abstraction by $H\dot{O}_2$ radical from EMK shows that the abstraction reaction channels are dominant over the entire temperature range of 600 – 1600 K.

Acknowledgments

This material is based upon works supported by Science Foundation Ireland under Grant No. [08/IN1./I2055]. Computational resources were provided by the Irish Center for High-End Computing, ICHEC. We thank Stephen J. Klippenstein for helpful discussions regarding the usage of Variflex verion 2.02m in the pressure dependent rate constants calculations.

Supporting Information

Supporting Information: Optimised geometries, rotational constants and vibrational frequencies of the species involved in the rate constant calculations computed at the MP2/6-311G(d,p) level (Table S1). This information is available via the Internet at http://pubs.acs.org.

References and Notes

[1] Beatrice, C.; Bertoli C.; Giacomo, N. D. New Findings on Combustion Behavior of Oxygenated Synthetic Diesel Fuels. *Combust. Sci. Technol.*, **1998**, *137*, 31-35.

[2] Wagner T.; Wyszynski, M.L. Aldehydes and Ketones in Engine Exhaust Emissions - A Review. *Proc. Inst. Mech. Eng.: J. Automob. Eng.*, **1996**, *210*, 109-122.

[3] Li, Y.; Wei, L.; Tian, Z.; Yang, B.; Wang, J.; Zhang T.; Qi, F. A Comprehensive Experimental Study of Low-pressure Premixed C-3-Oxygenated Hydrocarbon Flames with Tunable Synchrotron Photoionization. *Combust. Flame*, **2008**, *152*, 336-359.

[4] Zhou, C-W.; Simmie J. M.; Curran, H. J. Ab Initio and Kinetic Study of the Reaction of Ketones with OH for T = 500-2000 K. Part I: Hydrogen-Abstraction from H3CC(O)CH3Cx(CH3)x, x = 0 → 2 *Phys. Chem. Chem. Phys.*, **2011**, *13*, 11175-11192.

[5] Mendes, J. R.; Zhou C-W.; Curran, H. J. Theoretical and Kinetic Study of the Reactions of Ketones with HO2 Radical. Part I: Abstraction Reaction Channels *under review by J. Phys. Chem. A.*

[6] (a) Becke, A. D. Density-Functional Thermochemistry. I. The Effect of the Exchange-Only Gradient Correction. *J. Chem. Phys.*, **1992**, *96*, 2155-2160. (b) Becke, A. D. Density-Functional Thermochemistry. II. The Effect of the PerdewCWang Generalized-Gradient Correlation Correction. *J. Chem. Phys.*, **1992**, *97*, 9173-9177. (c) Becke, A. D. Density-Functional Thermochemistry. III. The Role of Exact Exchange.*J. Chem. Phys.*, **1993**, *98*, 5648-5652.

[7] Gonzalez, C.; Schlegel, H. B. An Improved Algorithm for Reaction Path Following. *J. Chem. Phys.*, **1989**, *90*, 2154-2161.

[8] (a) Baboul, A. G.; Curtiss, L. A.; Redfern, P. C.; Raghavachari, K. Gaussian-3 Theory Using Density Functional Geometries and Zero-point Energies. *J. Chem. Phys.*, **1999**, *110*, 7650-7657. (b) Curtiss, L. A.; Raghavachari, K.; Redfern, P. C.; Baboul, A. G.; Pople, J. A. Gaussian-3 Theory Using Coupled Cluster Energies. *Chem. Phys. Lett.* **1999**, *314*, 101-107.

[9] Frisch, M. J.; Trucks, G. W.; Schlegel, H. B.; Scuseria, G. E.; Robb, M. A.; Cheeseman, J. R.; Scalmani, G.; Barone, V.; Mennucci, B.; Petersson, G. A. *et al. Gaussian 09*, Gaussian, Inc.: Wallingford, CT, 2009.

[10] Werner, H.-J.; Knowles, P. J.; Lindh, R.; Manby, F. R.; Schütz, M.; Celani, M.; Korona, T.; Mitrushenkov, A.; Rauhut, G.; Adler, T. B. *et al. MOLPRO, Version 2010.1*, a package of ab initio programs; University College Cardiff Consultants Limited: Wales, U.K., 2009.

[11] Miller, J. A.; Klippenstein, S.J.; Raffy, C. Solution of Some One- and Two-dimensional Master Equation Models for Thermal Dissociation: The Dissociation of Methane in the Low-Pressure Limit. *J. Phys. Chem. A*, **2002**, *106*, 4904-4913.

[12] Miller, J. A.; Klippenstein, S.J. Master Equation Methods in Gas Phase Chemical Kinetics. *J. Phys. Chem. A* **2006**, *110*, 10528-10544.

[13] Eckart, C. The Penetration of a Potential Barrier by Electrons. *Phys. Rev.* **1930**, *35*, 1303-1309.

[14] Mourits, F. M.; Rummens, F. H. A. A Critical Evaluation of LennardCJones and Stockmayer Potential Parameters and of some Correlation Methods. *Can. J. Chem.*, **1977**, *55*, 3007-3020.

[15] Senosiain, J. P.; Klippenstein, S. J.; Miller, J. A. Reaction of Ethylene with Hydroxyl Radicals: A Theoretical Study. *J. Phys. Chem. A*, **2006**, *110*, 6960-6970.

[16] Klippenstein, S. J.; Wagner, A. F.; Dunbar, R. C.; Wardlaw, D. M.; Robertson, S. H.; Miller, J. A. *VARIFLEX Version2.02m*, 2010.

[17] Wang, J.; Li, Y.; Zhang, T.; Tian, Z.; Yang, B.; Zhang, K.; Qi, F.; Zhu, A.; Cui, Z.; Ng, C-Y. Interstellar Enols are Formed in Plasma Discharges of Alcohols. *Astrophys J*, **2008**, *676*, 416-419.

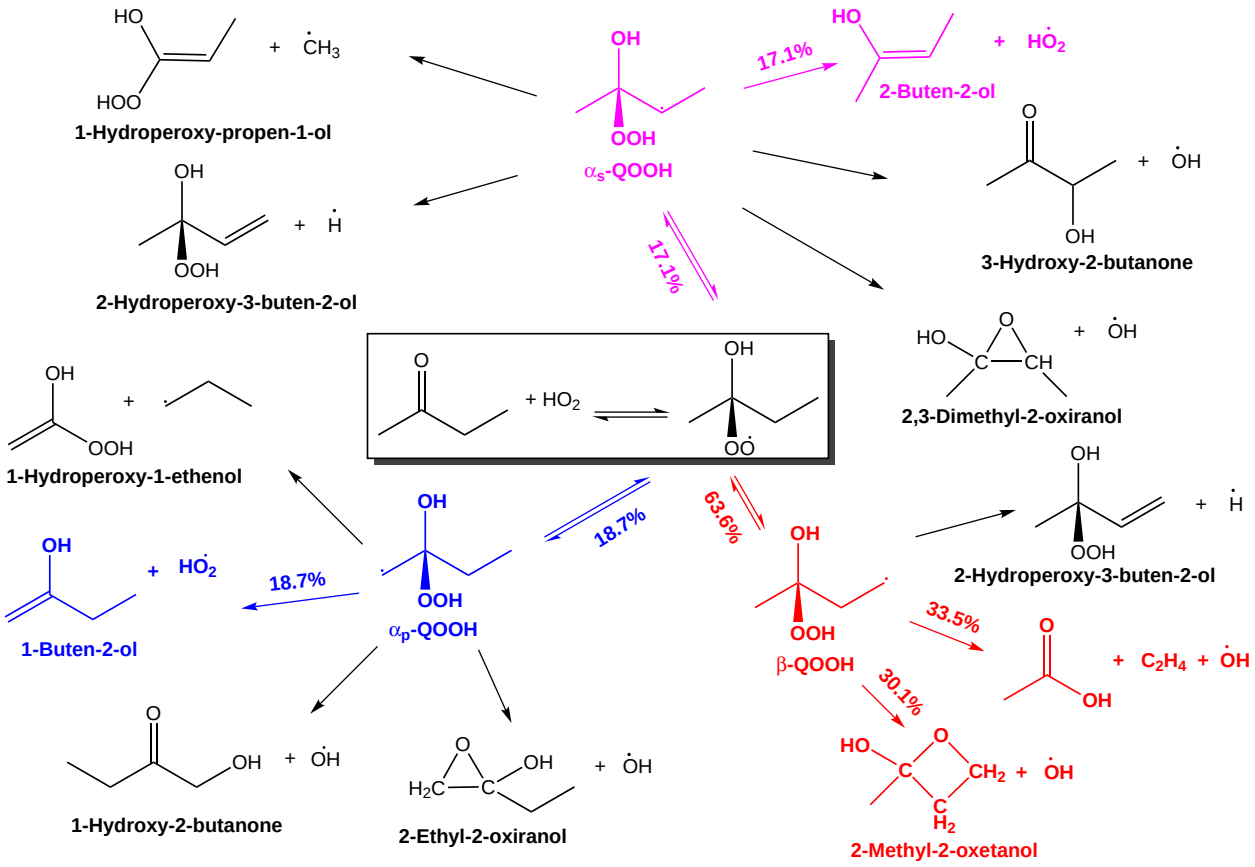

Figure 1: Reaction channels investigated in this work, numbers refer to a flux analysis based on rate constants calculated at 1000 K.

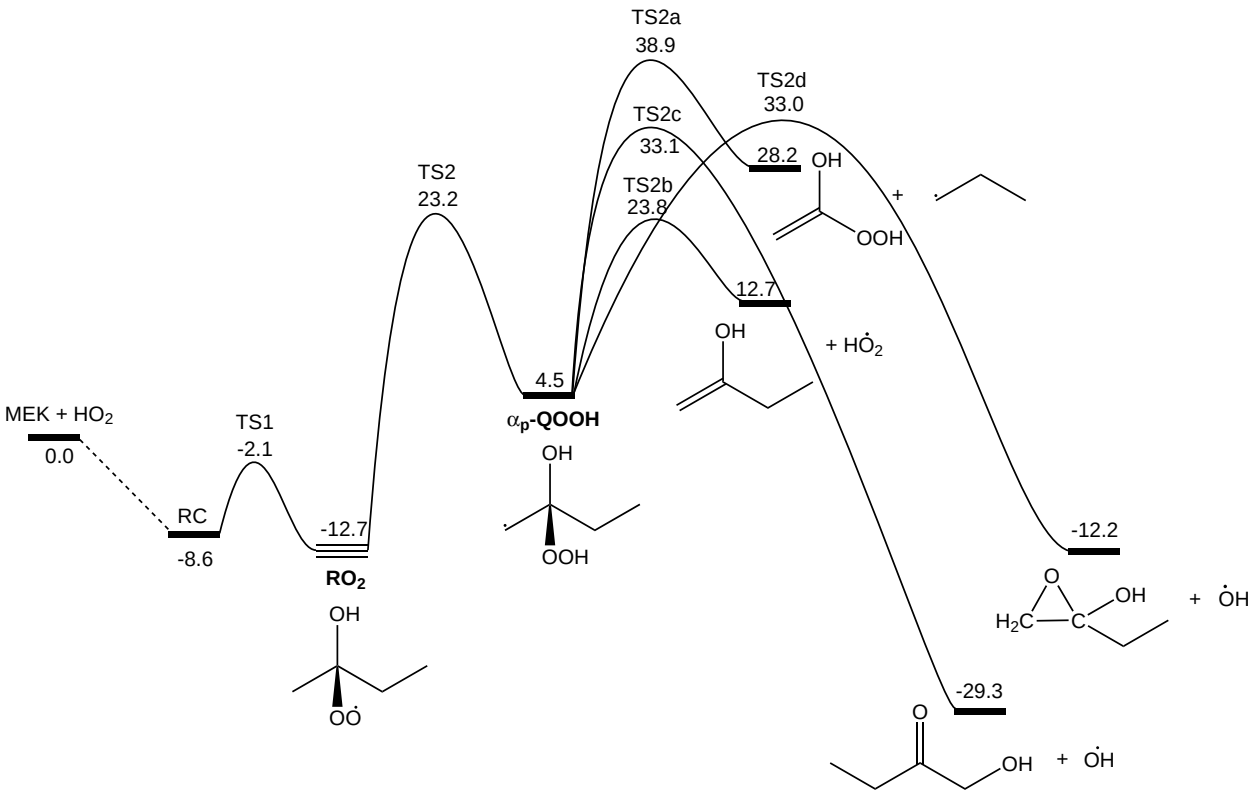

Figure 2: Potential energy diagram in kcal mol^{-1} for the formation and decomposition of α_{p}-Q̇OOH at G3(MP2,CC) level of theory.

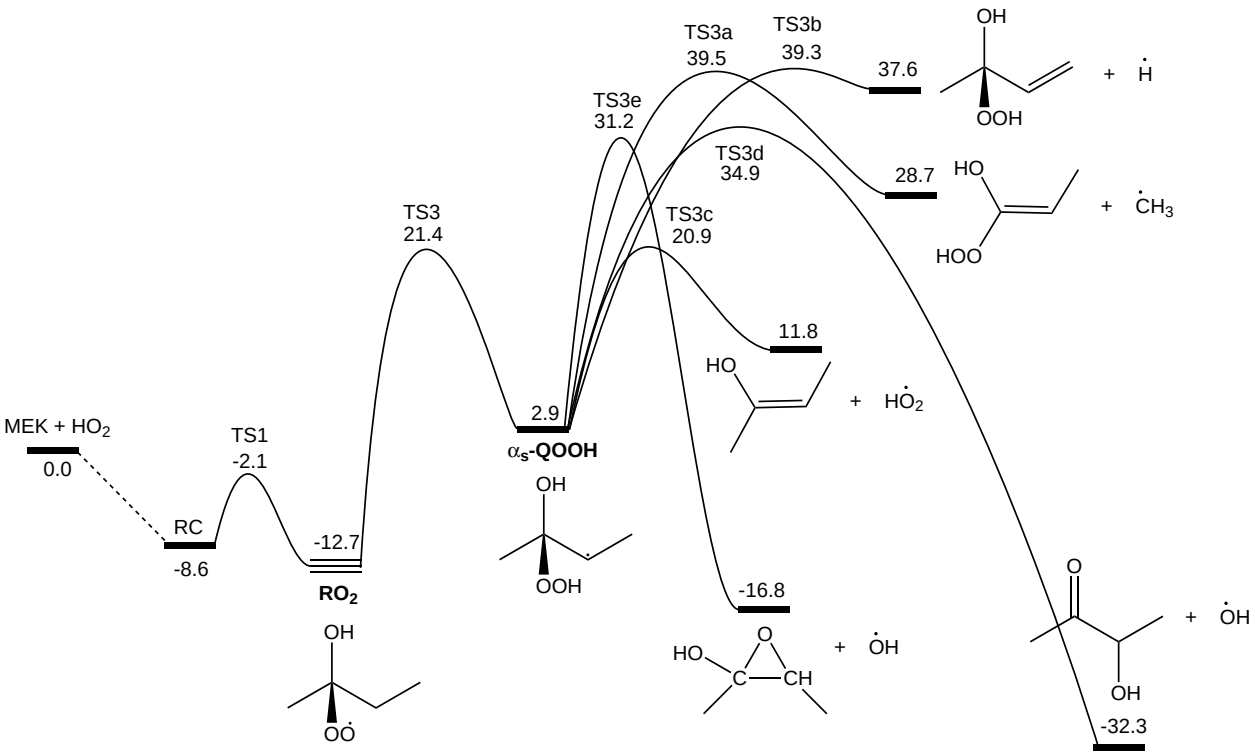

Figure 3: Potential energy diagram in kcal mol^{-1} for the formation and decomposition of α_s-Q̇OOH at G3(MP2,CC) level of theory.

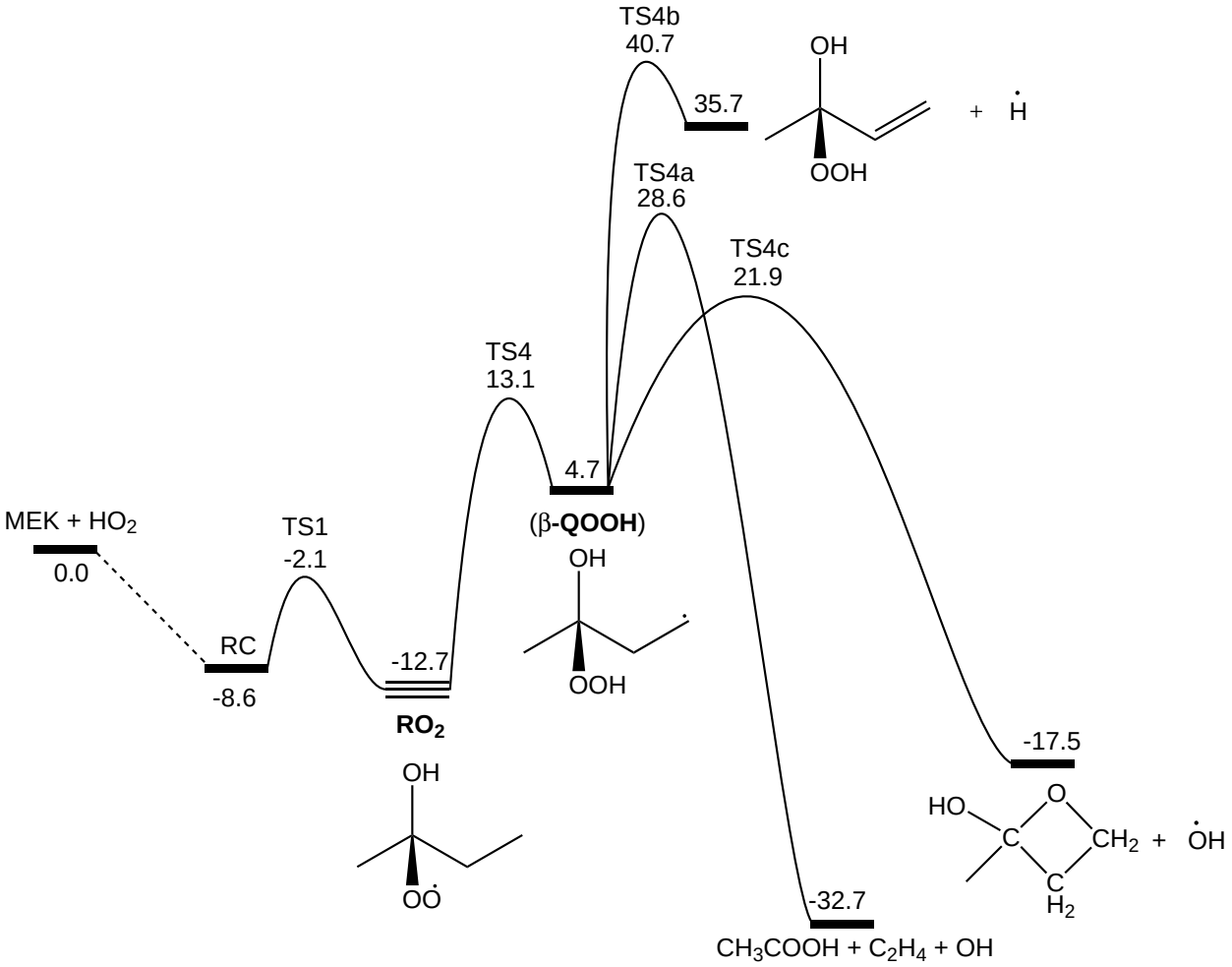

Figure 4: Potential energy diagram in kcal mol^{-1} for the formation and decomposition of β-$\dot{\text{Q}}$OOH at G3(MP2,CC) level of theory.

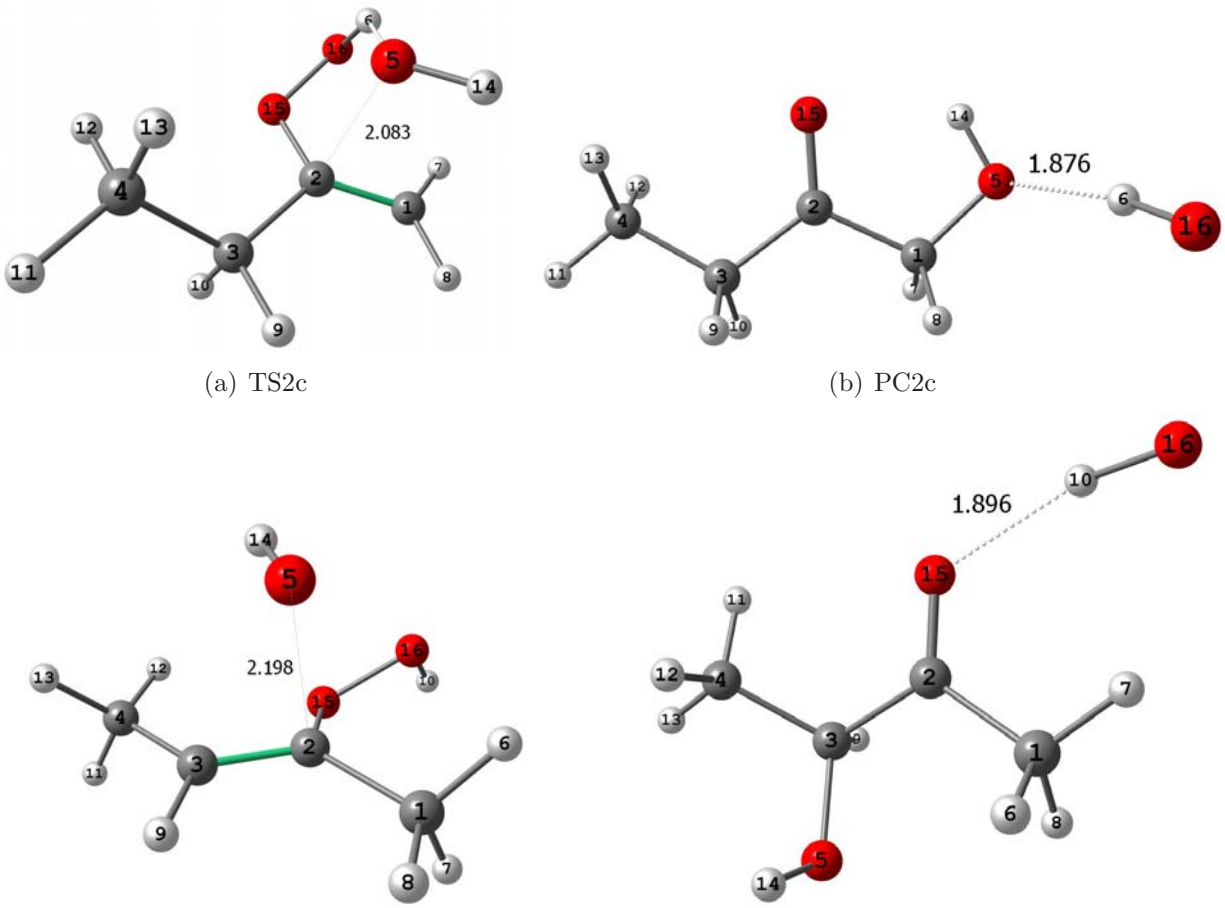

(a) TS2c (b) PC2c

(c) TS3d (d) PC3d

Figure 5: Optimized geometries of transition states and product complexes for the ȮH-elimination reaction channels in α_p-Q̇OOH and α_s-Q̇OOH at B3LYP/6-311G(d,p) level of theory.

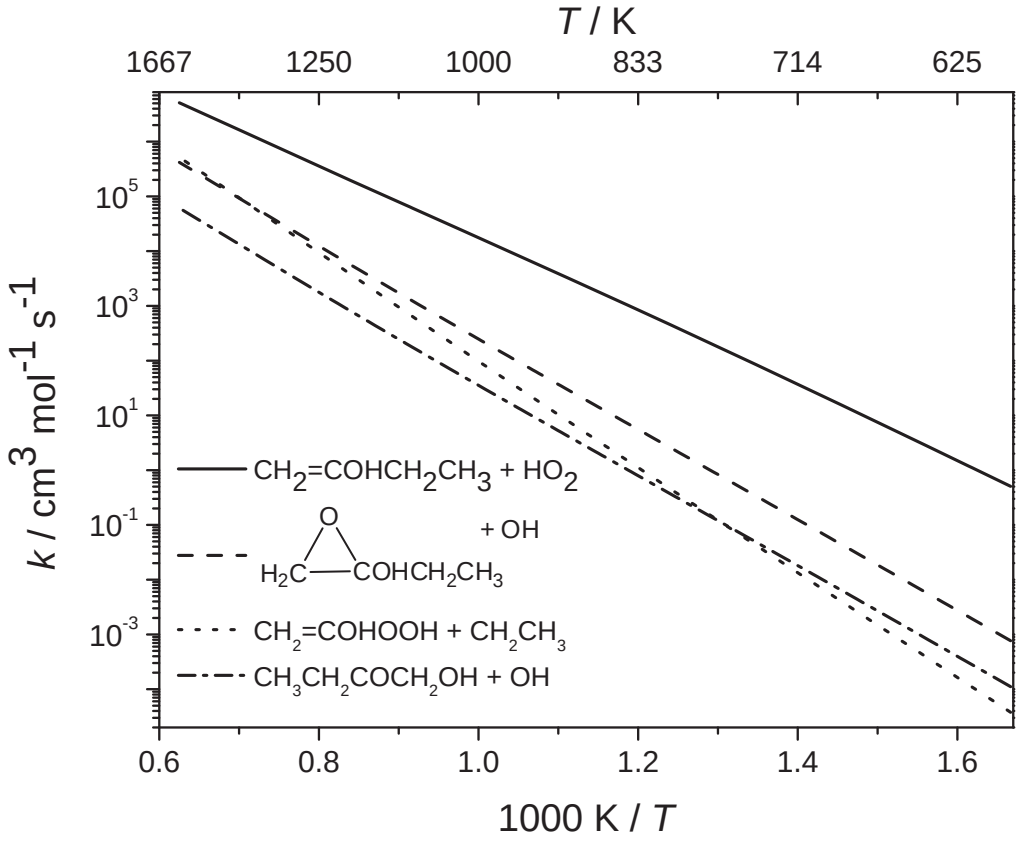

Figure 6: Bimolecular rate constants for comparison for the four major product channels in the decomposition of α_{p}-Q̇OOH at 1 atm.

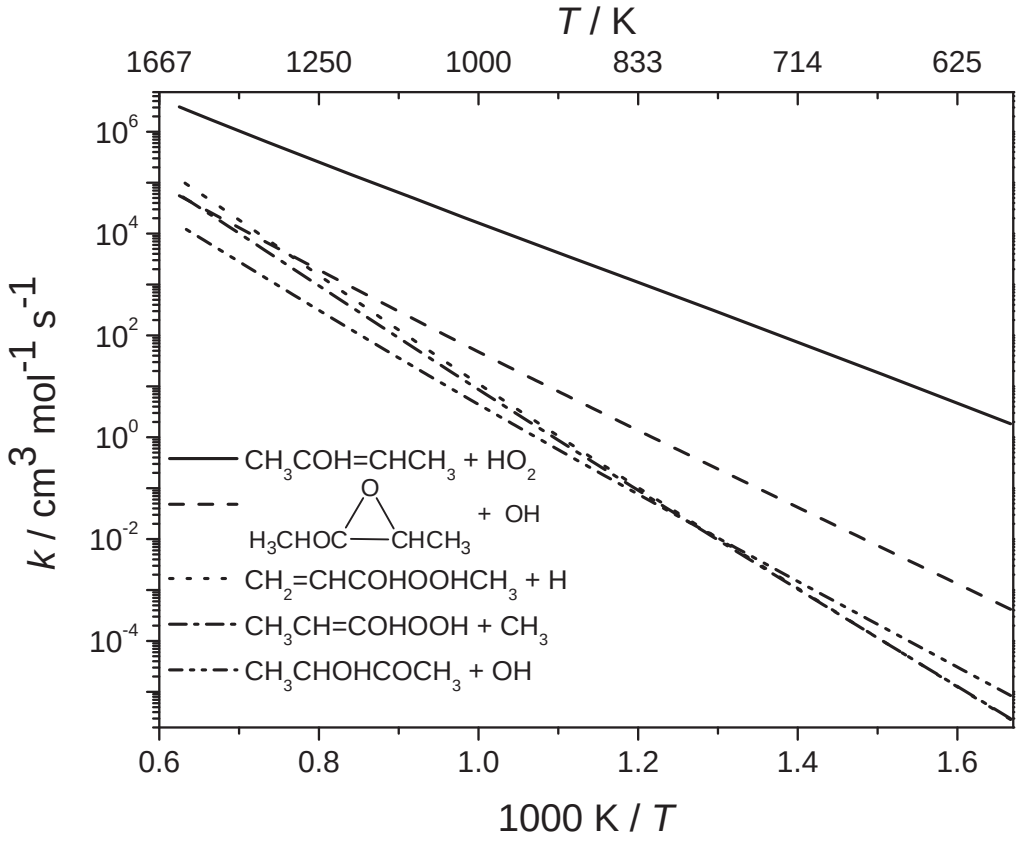

Figure 7: Bimolecular rate constants for comparison for the five major product channels in the decomposition of α_s-Q̇OOH at 1 atm.

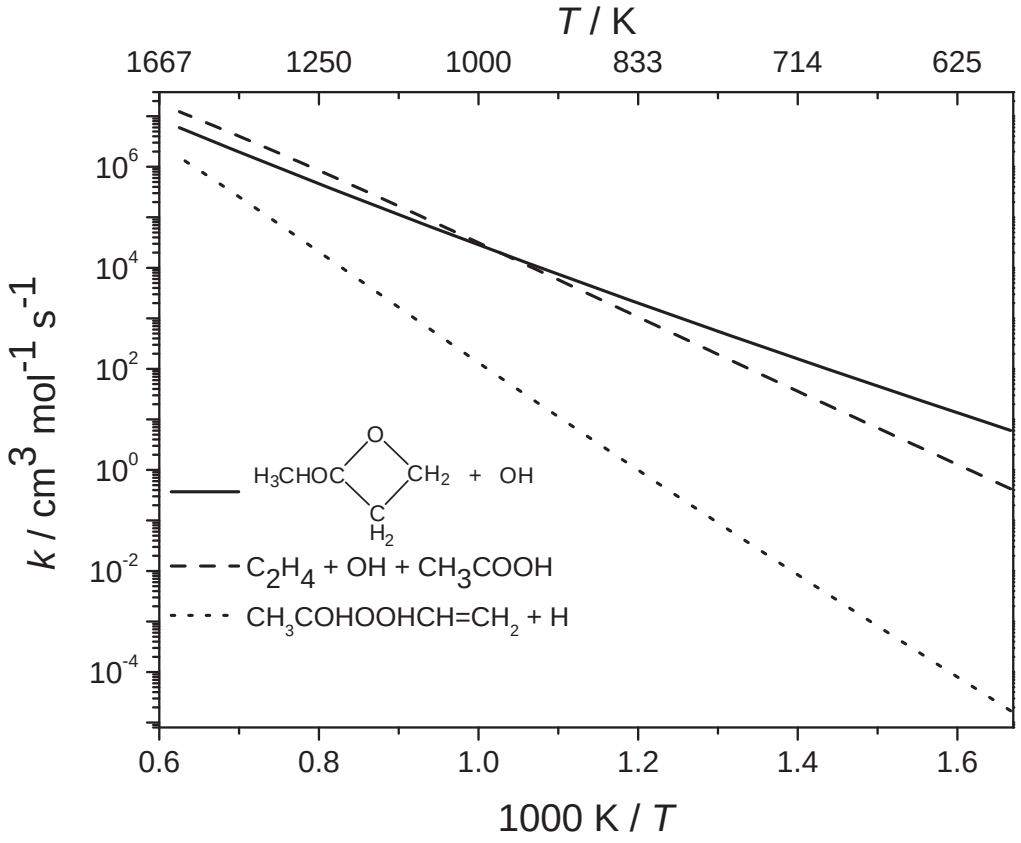

Figure 8: Bimolecular rate constants for comparison for the three major product channels in the decomposition of β-Q̇OOH at 1 atm.

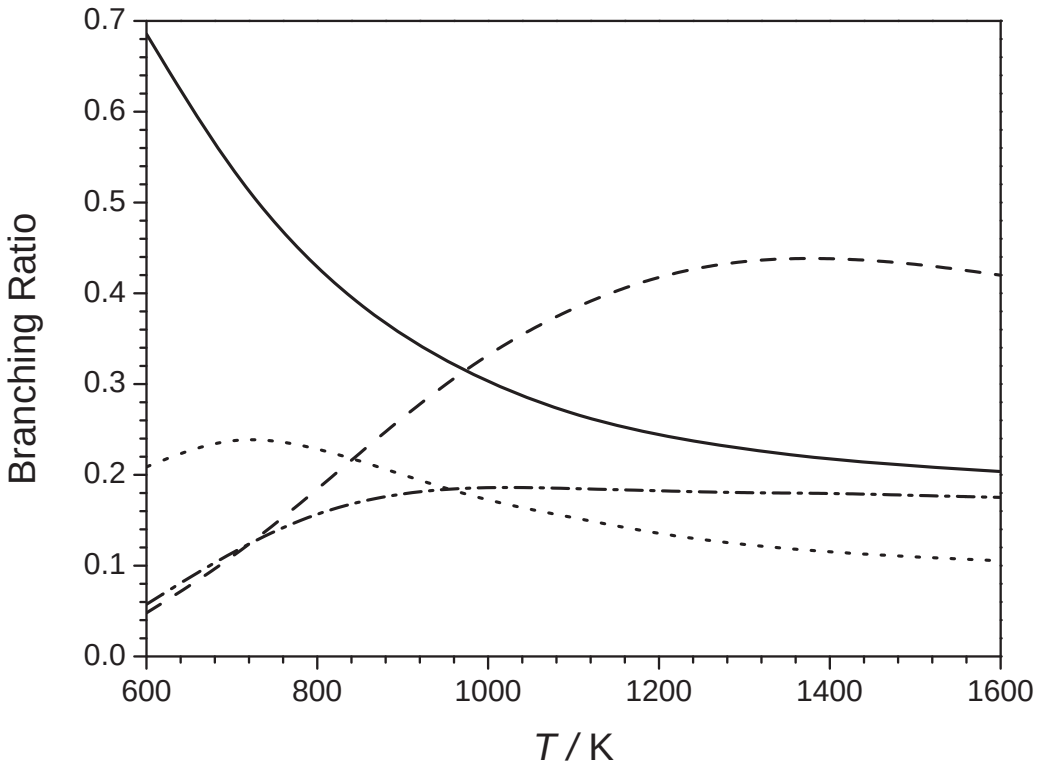

Figure 9: Branching ratio comparison at 1 atm for the formation of —— 2-methyl-2-oxetanol and $\dot{O}H$ radical; — — acetic acid, ethylene, $\dot{O}H$ radical; $\cdots$ 2-buten-2-ol and $H\dot{O}_2$ radical; and — $\cdot$ — 1-buten-2-ol and $H\dot{O}_2$ radical.

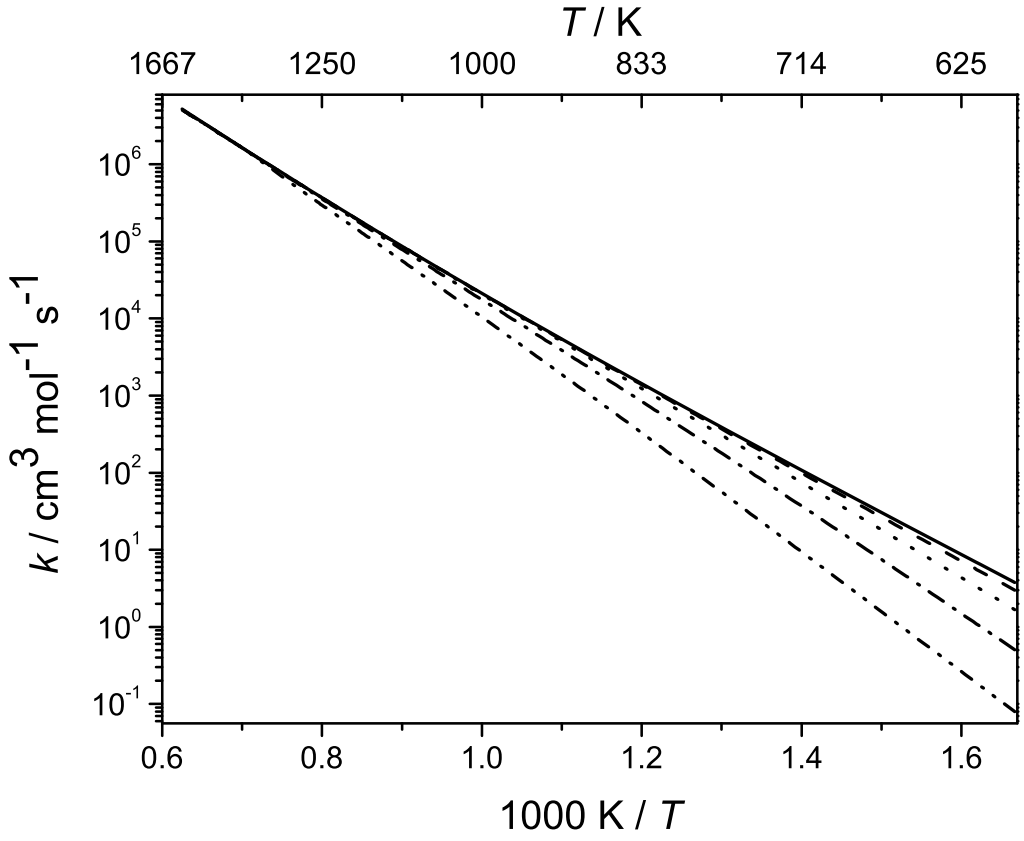

Figure 10: Pressure dependence rate constants comparison for the formation of 1-buten-2-ol and $H\dot{O}_2$ radical. ── collisionless limit, ─ ─ 0.01 atm, ··· 0.1 atm, ─ · ─ 1 atm and ─ · · ─ 10 atm.

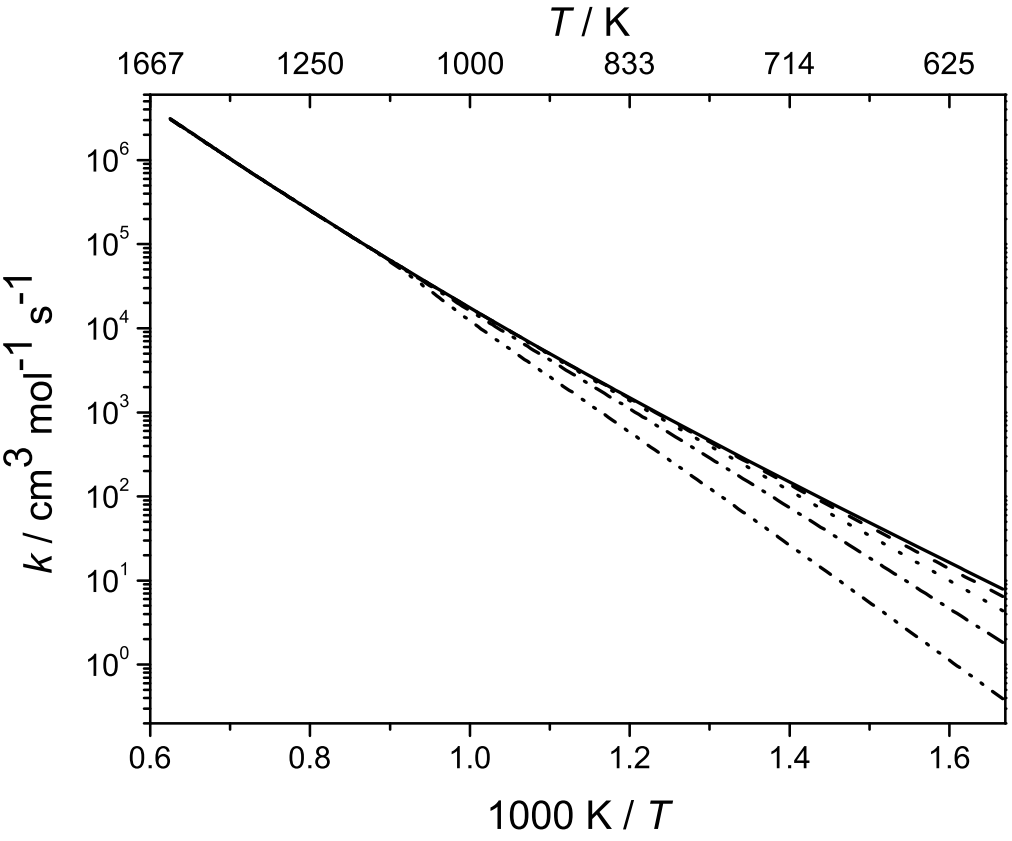

Figure 11: Pressure dependence rate constants comparison for the formation of 2-buten-2-ol and $H\dot{O}_2$ radical. ── collisionless limit, ─ ─ 0.01 atm, ··· 0.1 atm, ─ · ─ 1 atm and ─ · · ─ 10 atm.

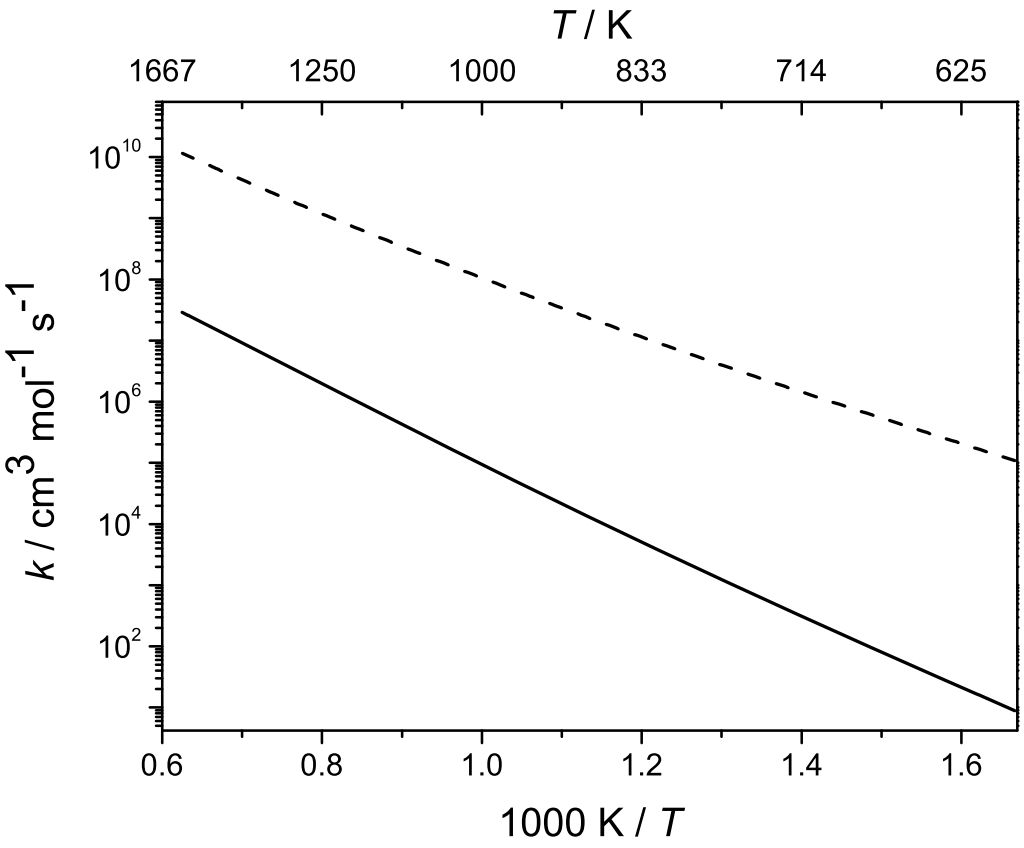

Figure 12: Total rate constants comparison for the addition of $H\dot{O}_2$ radical to EMK, —— this work, and for H-atom abstraction by $H\dot{O}_2$ radical from EMK,[5] — —.

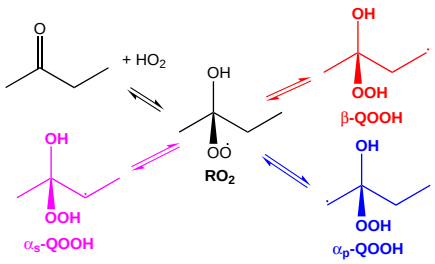

Figure 13: Table Of Content